

Sizing of FFR to Improve Frequency Security in Low-Inertia Power Systems

Savvas Panagi¹ and Petros Aristedou

School of Electrical and Computer Engineering, Cyprus University of Technology

¹Email: savvas.panagi@cut.ac.cy

Abstract—As more renewable energy sources join the power grid, the electric industry is dealing with problems like system inertia. However, using battery energy storage systems (BESS) helps address stability issues caused. This paper focused in low inertia power systems and proposed a simulation-based methodology for sizing FFR maximum power to improve frequency response and mainly Nadir. The proposed approach was evaluated in a Cyprus simplified power system, considering a variety of random power plant dispatch, PV generation, wind generation, and load consumption scenarios. DIGSILENT PowerFactory and Python programming language is used for developing, testing, and analyzing the system model. The results verified the fast model convergence and quite accurate results.

I. INTRODUCTION

In every electrical system, the generated power must precisely balance with the power consumed at any given moment. Any deviation from this equilibrium results in a power imbalance. Through the behavior of synchronous generators, power imbalance leads to changes in the electrical frequency of the system [1]–[3]. Power imbalances can arise in the system due to unexpected interruptions in production or consumption units, commonly referred to as disturbance imbalances. Fig. 1 illustrates a frequency response in different case studies where an instance of a loss of generation event occurs. Each transmission system operator is responsible for ensuring sufficient reserve to be within the grid-code regulation to avoid protection tripping and frequency instability. For this purpose, they define various system support products [4], [5]. ROCOF, Nadir, and post-fault frequency steady state were some but not the only important indices that must be considered in the design of frequency reserve products [6], [7].

Traditional power grids heavily rely on centralized power generation from large-scale power plants, and they primarily use synchronous generators (SGs) for frequency stability by providing inertia and frequency control [7]. Sustainability goals have imposed rules to decrease dependency on fossil fuels and tackle environmental issues, leading to an increase in inverter-based resource penetration. Hence, decommissioning of SGs reduces the inertia and frequency control capabilities and causes more significant frequency regulation issues, especially in low-inertia power systems [8]. Fig. 1 illustrates the impact of decreasing inertia on the system. As inverter-based resources increase, the Nadir after a generator fault rises. A survey between 12 synchronous system operators revealed that 80% expect that reducing inertia will cause frequency challenges [3]. Hence, involved parties are forced to investigate

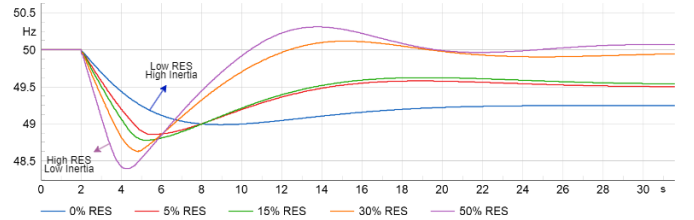


Fig. 1. Impact of decreasing inertia

novel methods and technologies to control and mitigate the frequency response and Nadir. Increasingly, more operators are introducing energy storage systems (ESS) to improve the frequency stability of their power systems. ESS can provide frequency reserves by replicating the operation of inertia and FCR. Nevertheless, these services are not targeted in Nadir and their implementation may be financially difficult. Hence, an increasing trend is observed where operators are incorporating Fast Frequency Response (FFR) reserves through ESS as a new support service. While establishing the required levels of inertia and frequency containment reserve (FCR) offers a foundational understanding through static analyses that employ the swing equation and the regulation factor of each power plant governor, achieving an enhanced fast-frequency response (FFR) requires a more intricate approach. As the Nadir is strongly non-linear and protection units are included in the power system, dynamic analyses become imperative to guarantee improvements in the Nadir.

As the complexities of power system stability unfold, the literature provides valuable insights into diverse methodologies for sizing and strategically placing Battery Energy Storage Systems (BESS) to enhance frequency response [9]–[17]. A lot of already published work is trying to dimension the optimal sizing of ESS based on optimization processes [9], [12], [14]–[16]. Fitness-scaled chaotic artificial bee colony optimization modeled and used in [9] to archive a targeted Nadir while minimizing ROCOF, three variables are decided after the optimization: BESS sizing (MW), and tuning parameters of the PQ controller related to the real power part (K_p and T_{ip}). To improve the Nadir, ROCOF, and voltage deviation through a multi-objective binary grey wolf optimization (GWO) approach, it is investigated in [14]. In [15] rated power of BESS (S_b) and the gain of a droop-based controller (K) were selected to minimize a cost function using the BAT optimization algorithm (BOA) within there is a constraint that

the nadir must be less than the point of 1st stage UFLS. The cost objective function is also used in [16], in which authors try to maximize the profit of the potential BESS owner based on historical frequency measurement data. In [12] GWO approach is used to determine BESS sizing while focusing on minimizing Nadir. In place of the optimization algorithm, an average value through 10,000 Monte-Carlo trials was proposed in [17] to analyze the behavior of Nadir and ROCOF. In [10], investigated step reduction iterative algorithm (SRIA) which dimension BESS size that provides FFR to regulate the frequency maximum deviation after an outage. In [13], a direct equation to calculate BESS size based on a reference outage event is proposed. An iteration method for a different BESS power is proposed in [11] where the optimal size is determined by two semi-empirical decisions: 1) increasing the BESS size does not provide significant improvement, and 2) based on BESS maximum discharge power efficiency.

Most of the above works focus on FCR and IR provision from BESS, which requires a large capacity of the storage unit and, by extension, higher costs. Moreover, until the convergence of most optimization algorithms, a large computing cost will be needed. Extremely high computing costs are also needed in the iteration method, which tries to combine all possible BESS sizes to reach the optimum. A gap is also observed through analytical dimension methodologies because several assumptions are made and protection schemes cannot be implemented in those analyses. In addition, some of the analyses focused on the improvement of frequency response without targeting a specific Nadir point. On the other side, the current work combines the utilization of a simulation model and a BESS power sizing estimator method to archive the target of Nadir. The algorithm started with a fairly good initial approach to the requirement of FFR, which gives the ability for faster convergence. This work focuses on FFR auxiliary frequency service support dimensioning, which usually takes around 30 seconds of full power injection and, by extension, reduces energy needs and implementation costs.

The contributions of this paper are:

- A novel data-driven simulation-based algorithm for sizing FFR needs to achieve a targeted Nadir. The methodology can also be applied to low-inertia systems where various other protective methods, such as UFLS exist.
- Insights on the interaction between Inertia, FFR, FCR, and Nadir

This paper is structured as follows: In section II a brief explanation of frequency response and control is given. Section III discusses the proposed framework. The results are analyzed in section IV.

II. BACKGROUND

A. Frequency Control

The correction of the power balance and, therefore, the frequency response shall be made in a hierarchical manner, where each control stage is separated from the subsequent stages. In the initial stage, the inertia response takes action, with a response time of fractions of milliseconds (ms) that retains the rate of change of frequency (ROCOF) [18]. Following this, the

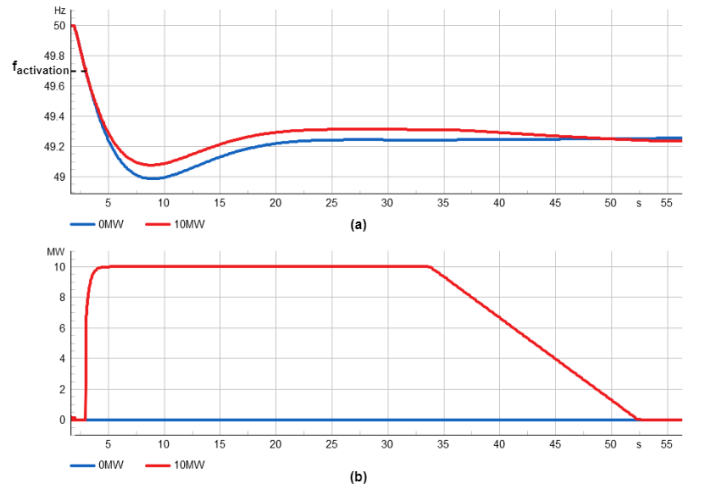


Fig. 2. FFR in Disturbance event

fast frequency response (FFR) is swiftly engaged to provide additional support, ensuring a rapid adjustment and reducing Nadir [19]. In the next stage, the frequency containment reserve (FCR) comes into play with a response time of a few seconds, aiming to stabilize the frequency [6]. In the third stage, the frequency restoration reserve (FRR) with a response time of several minutes is employed to restore the frequency to its nominal value. Finally, there is the replacement reserve (RR), to restore the available reserve to initial levels and prepare the system for new frequency deviations [2], [6], [20].

B. Frequency Reserve Products

Inertia: In power systems, inertia refers to the energy stored in large rotating generators and certain industrial motors. This stored energy can be particularly valuable in situations of power imbalance [21], [22]. Lower system inertia can lead to increased frequency sensitivity in cases of disturbances, as any change in power balance has a more immediate impact on frequency due to the limited inertia [18].

FFR: The goal of FFR is to provide a very fast reserve due to disturbances and frequency changes in the network by adding power to the grid, aiming to reduce the Nadir [19], [22]. The FFR is capable of reacting in a very short time frame, usually less than 1 second [22]. FFR functions as a complement to FCR_D and inertia but does not alleviate the minimum needs for these reserves and thus cannot replace them [21]. Figure 2a represents how FFR affects Nadir but does not affect the ROCOF and post-fault frequency steady-state, which confirms the non-replacement of FCR and inertia. There are several implementations of the FFR each offering unique perspectives. Some of these methodologies are presented in [3] and [22]. In line with the analysis conducted by EirGrid and NEM, a step response signal will be employed in the current analysis [22]. Figure 2b illustrates the BESS response behavior upon receiving an FFR activation signal.

FCR: The scope of FCR is to restrain the network's frequency within predefined levels [19] and is divided into FCR_D and FCR_N . The frequency containment reserve

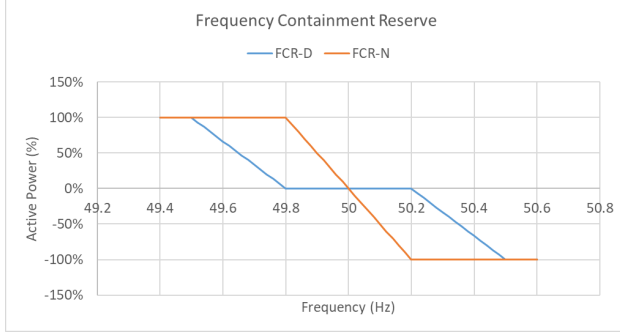


Fig. 3. *FCR* operation model

(FCR) for disturbances refers to a reserve enabled during a significant reduction in frequency caused by a sudden change in power. The reserve is activated within a few seconds, and its duration can last from 15 to 30 minutes, depending on the system's technical characteristics [23]. FCR_D activated linearly within the maximum frequency deviation range with a deadband at the normal frequency range. It is an asymmetric product, meaning it defines separately upward and downward reserve needs [24]. Figure 3 with blue line illustrates the operation mode based on the nominal capacity of FCR_D if we consider that maximum post-fault frequency deviation ± 0.5 Hz. FCR_N refers to a reserve energy source maintained to ensure the stability of the electrical network's frequency during its normal frequency deviation without significant disturbances. It is linearly activated within the normal frequency range [19] and is a symmetrical product [24], [19]. Figure 3 with orange line illustrates the operation mode based on the nominal capacity of FCR_N if we consider that normal frequency deviation was equal to ± 0.2 Hz.

FRR: Frequency Restoration Reserve is divided into aFRR and mFRR. The automatic FRR refers to a compensation system that is automatically activated to restore the frequency of the electrical network to its nominal value [4]. The primary purpose of aFRR is to address brief and unpredictable energy imbalances [25]. The aFRR was an asymmetrical product [19]. The manual FRR refers to power reserves that are manually activated by responsible entities to restore the frequency in case of imbalances, and it is also an asymmetrical product [4], [19]. The manual Frequency Restoration Reserves (mFRR) function to offset exceptionally widespread energy imbalances [25].

RR: The replacement reserve is available within a few minutes, and its purpose is to provide the desired amount of power to the system so that a) the electricity supply to consumers who may have been disconnected from the system is restored and b) the reserves that have been committed released, ensuring readiness to address any potential future frequency imbalance events. It is utilized only when all other energy balancing reserves have been activated [6], [20].

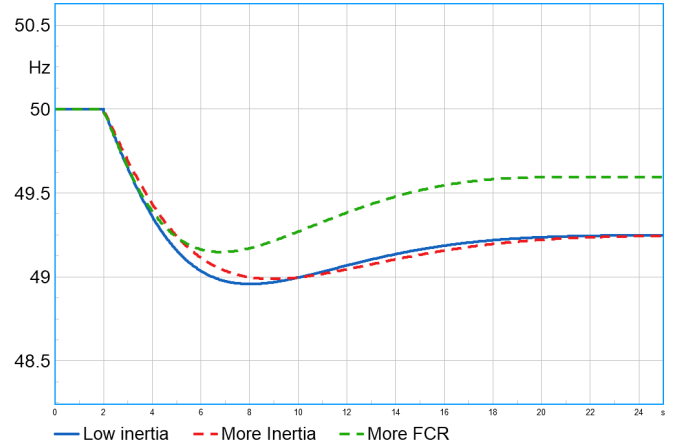


Fig. 4. Frequency Response in Different Operating Conditions [7].

C. Under Frequency Load Shedding

UFLS protection includes two different types of load reduction: a) demand response and b) necessary load shedding. These load disconnections occur when the available reserves are insufficient to restrain and restore the frequency within acceptable limits [26]. Various stages of UFLS are defined, with each stage progressively disconnecting different segments of the load. Low inertia systems suffer from increased UFLS situation as they now continuously lead to load disconnections, which increasingly affects the reliability of the system. It is worth noting that this process is considered undesirable due to the negative socio-economic impacts it causes.

D. Control interaction between Inertia, FFR, FCR and Nadir

Apart from ROCOF and post-fault frequency steady-state requirements, Nadir is an important parameter to examine, especially in low-inertia systems during disturbances. The drop of frequency may lead to unwanted events, e.g. UFLS activation. Based on these conditions, TSOs are required to consider inertia, FCR response time, FCR capacity, and FFR during significant imbalance events [7]. During a loss of power, systems with equal inertia show better performance with more FCR reserve, even though ROCOF is not affected. A decrease of Nadir is also observed with the increase in kinetic energy (Inertia). This observation is shown in Fig. 4.

To analyse how FCR response time, FCR capacity, and inertia affect the Nadir, a dynamic assessment of the power system for different operation scenarios is needed. For instance, Fig. 5a represents with green dots the analysed scenarios where Nadir is greater than 49 Hz when no FFR is available. Figures 5b and 5c illustrate the impact of incorporating an FFR of 10 MW and 20 MW, respectively. Comparison with Fig. 5a reveals a reduction in the requirements for kinetic energy and FCR when a higher FFR is available.

Finally, as depicted in Fig. 5, some scenarios with the same inertia and less FCR capacity may result in a higher Nadir due to the faster response time of the available FCR units.

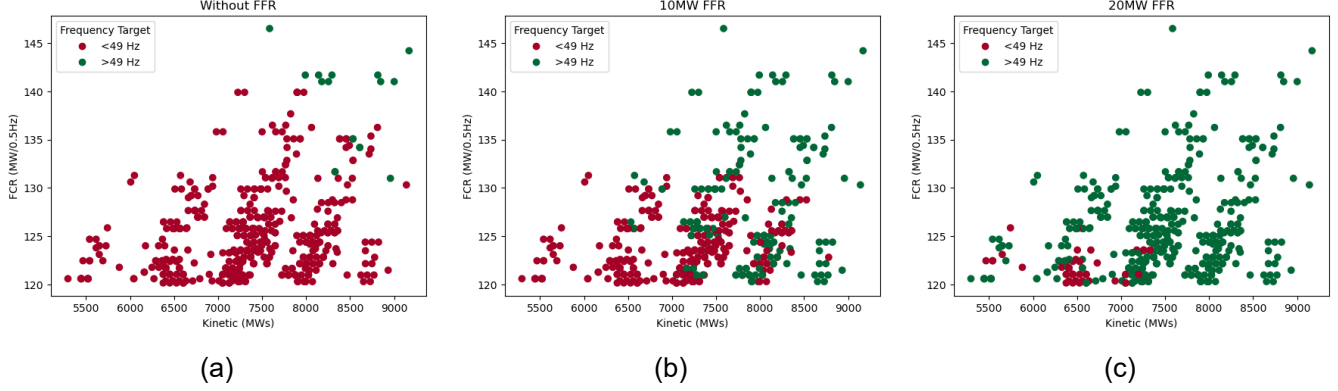


Fig. 5. kinetic energy and inertia ratio to meet Nadir requirements of 49Hz with FFR implemented.

E. Sizing minimum required kinetic energy (inertia) to meet ROCOF requirements

The kinetic energy is necessary to restrict the ROCOF (expressed in Hz/s) after the loss of generation. To compute the necessary kinetic energy to satisfy the ROCOF requirements, we employ the following equation [22]:

$$\text{ROCOF} = \frac{\Delta P}{2} \cdot \frac{f_n}{\sum_{i=1}^N H_i \cdot S_{n_i}} = \frac{\Delta P}{2} \cdot \frac{f_n}{E_{\text{kin}}} \quad (1)$$

where:

- E_{kin} is the post-fault kinetic energy,
- ΔP is the power imbalance occurred,
- f_n is the nominal frequency.

Which leads to the required kinetic energy computed as:

$$E_{\text{kin,req}} = \Delta P_{\text{max}} \cdot \frac{f_n}{2 \cdot \text{ROCOF}_{\text{max}}} \quad (2)$$

with $E_{\text{kin,req}}$ the total post-fault required kinetic energy to archive the maximum accepted ROCOF ($\text{ROCOF}_{\text{max}}$) and ΔP_{max} is the maximum power imbalance in the system. It should be noted that the kinetic energy requirement does not include the kinetic energy offered by the disconnected unit.

F. Sizing minimum required FCR_D^+ to meet post-fault frequency steady state after disturbances

For sizing the FCR_D^+ requirements, we must consider at least the loss of the largest power production unit. Thus, the required upwards frequency regulation coefficient (λ^+) can be computed with [3], [23]:

$$\lambda^+ = \frac{\Delta P_{\text{max}}}{\Delta f_{\text{max}}} = L_R + G_R \left[\frac{\text{MW}}{\text{Hz}} \right] \quad (3a)$$

where:

- ΔP_{max} is the maximum power imbalance occurred,
- Δf_{max} is the maximum accepted post-fault frequency deviation,
- L_R is the load regulation (self-load power adjustment),
- G_R is the generator regulation (FCR provided by generators).

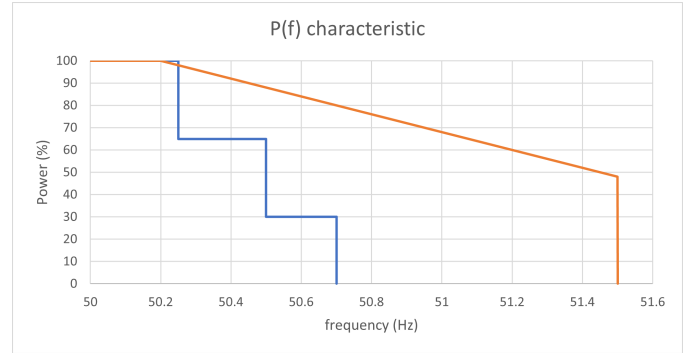


Fig. 6. Cyprus PV's and Wind Park frequency regulation characteristic [?], [27]

For, sizing FCR_D^- must take into account at least the maximum potential loss of load consumption unit. Thus, the required downwards frequency regulation coefficient (λ^-) can be computed with:

$$\lambda^- = \frac{\Delta P_{\text{max}}}{\Delta f_{\text{max}}} = L_R + G_R + PV_R + W_R \left[\frac{\text{MW}}{\text{Hz}} \right] \quad (3b)$$

where:

- PV_R is the photovoltaic regulation,
- W_R is the wind park regulation.

Except of load regulation and generator regulation, λ^- consider also photovoltaic regulation and wind regulation. All TSOs apply a protection policy for over-frequency situations for the safety of the system. Therefore, the production from renewable energy sources varies according to the grid's frequency. An example of PVs and wind regulation in the Cyprus power system is presented in figure 6.

III. PROPOSED ESS SIZING FOR FFR SERVICES

This section introduces the proposed data-driven approach for determining the optimal size of a BESS for FFR, an overview of which is shown in Fig. 7. The methodology requires the availability of a dynamic simulation model of the analysed system and historical information on the operating

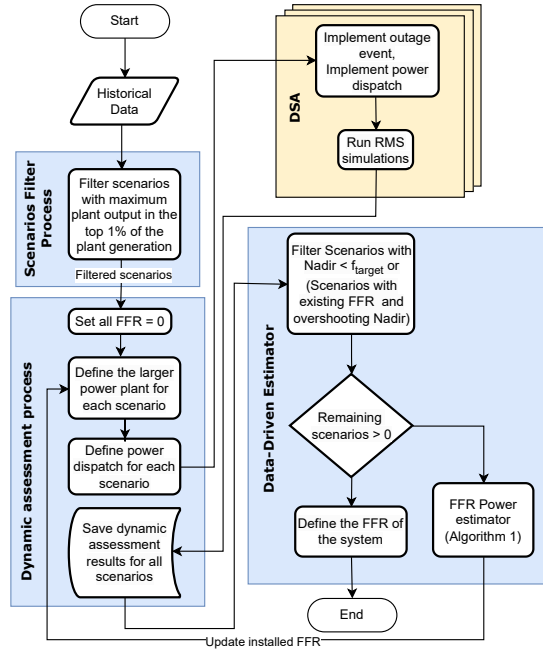


Fig. 7. Proposed methodology for FFR sizing

scenarios over at least one year. The target of this algorithm is to employ an iterative method that will compute the required FFR BESS size, for each scenario, that will lead a Nadir frequency close to the lowest accepted (named f_{target} below).

First, a filtering process is applied, keeping only the operating conditions where the maximum power plant operates in the top 1% of all the maximum generation outputs over all the data points. For each of the remaining scenarios, the data is used to initialise the dynamic simulation model and set up the contingency analysis.

Then, a Dynamic Security Assessment (DSA) is performed, simulating all the scenarios and extracting information on the frequency evolution (Nadir, ROCOF, post-fault steady state frequency, FCR activation speed). The DSA is embarrassingly parallel and can be implemented using multicore hardware to accelerate the simulation time. It is important to note that during this analysis, all frequency-related protection schemes (e.g., UFLS) that are not accepted in the sizing must be disabled to not affect the frequency response.

After the DSA, all scenarios with Nadir less than f_{target} or with existing FFR and Nadir exceeding 0.1% of f_{target} , are filtered. These are the scenarios where the FFR is either not adequate to bring the Nadir to f_{target} or bigger than necessary, thus overshooting the f_{target} .

While there are scenarios violating the requirements set in the previous paragraph, the required FFR is calculated using the FFR power estimator in Algorithm 1. After the process is completed, we extract the minimum and maximum FFR requirements over all the analysed scenarios.

A. FFR Power Estimator without UFLS activation

In this section, we explain the calculation of the FFR in Algorithm 1 when the activation of UFLS is not allowed. That

Algorithm 1: Data-Driven FFR estimator for each scenario

Data: Filtered scenarios
Result: FFR requirements for each scenario

- 1 **if not consider UFLS then**
- 2 \lfloor Calculate FFR based on (4);
- 3 **else**
- 4 \lfloor Calculate FFR based on (6);

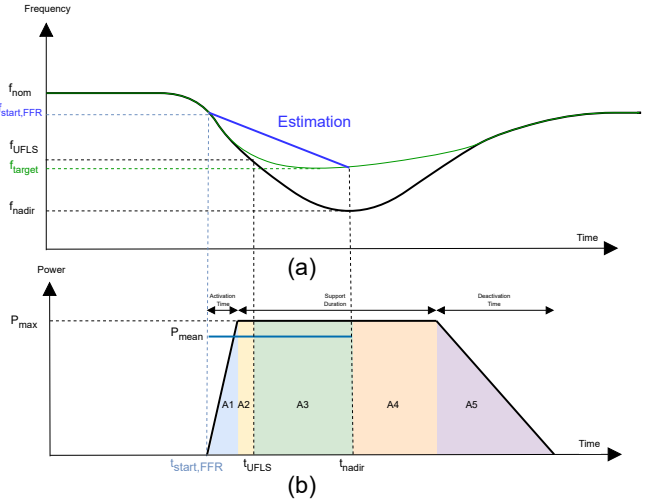


Fig. 8. FFR estimator approach

is, we assume that the f_{target} is higher than the first UFLS activation setpoint.

In the first iteration, the FFR is set to zero during the DSA, the following equations are used to estimate the required FFR values for the next iterations:

$$\Delta P_{FFR,mean,i} = \Delta P - \frac{f_{start,FFR} - f_{target}}{t_{nadir} - t_{start,FFR}} \cdot 2 \cdot \frac{E_{kin}}{f_n} - \quad (4a)$$

$$P_{FFR,mean,i-1} - P_{reg,load,mean} - P_{FCR,mean,i}$$

$$P_{FFR,max,i} = \Delta P_{FFR,mean,i} \cdot \frac{t_{nadir} - t_{start,FFR}}{t_{nadir} - t_{start,FFR} - \frac{T_{max,FFR}}{2}} + \quad (4b)$$

$$P_{FFR,max,i-1}$$

Equation 4a was formed based on Fig. 8a which illustrates with a blue line the linear frequency estimation approach that is used to estimate the required FFR . The previous simulation response is shown in black in the same figure, while the green line represents the frequency response after the computed FFR is updated in the dynamic model.

Equation 4b as presented in Fig. 8b convert the mean estimate FFR power to the maximum value used in the sizing. This can be done using an integral of the function over a given interval and then dividing by the length of that interval. In the current scenario, mean value was equal to the areas A1, A2,

and A3 divided by the corresponding interval time.

$f_{\text{start,FFR}}$ is the FFR activation frequency,

$t_{\text{start,FFR}}$ is the FFR activation time,

$P_{\text{FCR,mean,i}}$ is the average FCR,

$P_{\text{reg,load,mean}}$ is the average self-load regulation

The average load self-regulation was calculated between the activation of FFR frequency and the targeted frequency by the following equation:

$$P_{\text{load,reg,mean}} = \frac{(f_n - f_{\text{start,FFR}}) \cdot k \cdot \text{Load} + (f_n - f_{\text{target}}) \cdot k \cdot \text{Load}}{2} \quad (5)$$

Where:

k is the load self-regulation coefficient,

Load is the total load consumption,

B. FFR Power Estimator with first-stage UFLS activation

When one stage of UFLS is considered in the system, the following equations are used:

$$\frac{f_{\text{start,FFR}} - f_{\text{start,UFLS}}}{t_{\text{start,UFLS}} - t_{\text{start,FFR}}} = \frac{f_n}{2 \cdot E_{\text{kin}}} \cdot (\Delta P - P_{\text{FFR,i-1,mean,a}} - P_{\text{load,reg,mean,a}} - P_{\text{FCR,i,mean,a}} - \Delta P_{\text{FFR,mean,a}}) \quad (6a)$$

$$\frac{f_{\text{start,UFLS}} - f_{\text{target}}}{t_{\text{nadir}} - t_{\text{start,UFLS}}} = \frac{f_n}{2 \cdot E_{\text{kin}}} \cdot (\Delta P - P_{\text{FFR,i-1,mean,b}} - P_{\text{load,reg,mean,b}} - P_{\text{FCR,i,mean,b}} - P_{\text{UFLS}} - \Delta P_{\text{FFR,mean,b}}) \quad (6b)$$

Where:

$$P_{\text{load,reg,mean,a}} = \frac{(2 \cdot f_n - f_{\text{start,FFR}} - f_{\text{start,UFLS}}) \cdot k \cdot \text{Load}}{2} \quad (7a)$$

$$P_{\text{load,reg,mean,b}} = \frac{(2 \cdot f_n - f_{\text{start,UFLS}} - f_{\text{target}}) \cdot k \cdot \text{Load}}{2} \quad (7b)$$

$$P_{\text{UFLS}} = \text{Load}_{\text{shed,\%}} \cdot P_{\text{total,load}} - P_{\text{Vshed,\%}} \cdot P_{\text{total,PV}} \quad (7c)$$

$$\Delta P_{\text{FFR,mean,a}} = \frac{(t_{\text{start,UFLS}} - t_{\text{start,FFR}} - \frac{T_{\text{max,FFR}}}{2})}{t_{\text{start,UFLS}} - t_{\text{start,FFR}}} \cdot \Delta P_{\text{FFR,max}} \quad (7d)$$

$$\Delta P_{\text{FFR,mean,b}} = \Delta P_{\text{FFR,max}} \quad (7e)$$

$$P_{\text{FFR,i,max}} = P_{\text{FFR,i-1,max}} + \Delta P_{\text{FFR,max}} \quad (7f)$$

P_{UFLS} is the disconnected power taking consider PV's power disconnection from distribution system. $P_{\text{FFR,i-1,mean,a}}$ is the FFR average power of the previous iteration from the activation point of FFR until UFLS. $P_{\text{FFR,i-1,mean,b}}$ is the FFR average power of the previous iteration from UFLS until Nadir.

Equations (6a), (6b) use the same estimation approach as (4a) but divide the frequency response into two time segments. In the first segment (6a) describes the frequency response prior UFLS activated and the second (6b) describes the frequency response from the time that UFLS activated until the nadir.

To define the FFR maximum power in every iteration, (6a),(6b) solved in terms of $P_{\text{FFR,i,max}}$.

When in a power system more than one UFLS stages is accepted the equations (6), are modified similarly by dividing into more time segments.

C. BESS Power and Energy sizing

After completing the methodology, we define the maximum FFR requirements over all the analyzed scenarios. In order to sizing the energy capacity of the BESS needs to provide this power, Fig 8b curve adapted to corresponding grid codes.

IV. TEST RESULTS

A. Test System

The proposed approach was tested on the Cyprus power system, the single-line diagram shown in Fig. 9. Cyprus's power system consists of 26 generators, between steam, gas, and diesel power plants. Furthermore, 155 MW of wind farms and 610 MW of photovoltaic system capacity were installed. The minimum load demand based on historical data was 300 MW, and the maximum load was around 1240 MW.

The dynamic model was developed in DiGSILENT Powerfactory software and contains, apart from the above, 13 under-frequency load shedding (UFLS) stages and the proposed BESS with FFR implementation.

B. Parameters and Implementation

As the historical data of the Cypriot system does not cover the necessary needs for a minimum FCR and inertia requirements, random scenarios have been created where the STG7 is constantly at the maximum operating power of 120 MW, and after 1 second of normal operation it suddenly disconnects from the network by opening the switch breaker of this plant. The limits of each generator power operation are given in Table I. Minimum inertia was calculated to keep the ROCOF within the requirement limit of 1Hz/sec. Under frequency load shedding scheme which is implemented in Cyprus represented in Table II, where at the same time as load shedding, the corresponding percentage of PV installed in the distribution network is also disconnected. In Table. III all considered simulated parameters are defined.

TABLE I
GENERATORS POWER DISPATCH RANGE

Generator	Max Power (MW)
GTG1-GTG5	20
DG1-DG6	15
CCGT-STM1	35
CCGT-STM2	35
GAS1-GAS4	45
STG1-STG6	45
STG7	120
STG 8-9	105

C. Results without UFLS

In this test case, UFLS is not accepted in the system, so the frequency target was set to 49 Hz. Firstly, a simulation of the 500 random scenarios was established, and only 15 scenarios had a frequency greater than the target. The Fig. 10a represents the results after the first iteration where BESS is not activated.

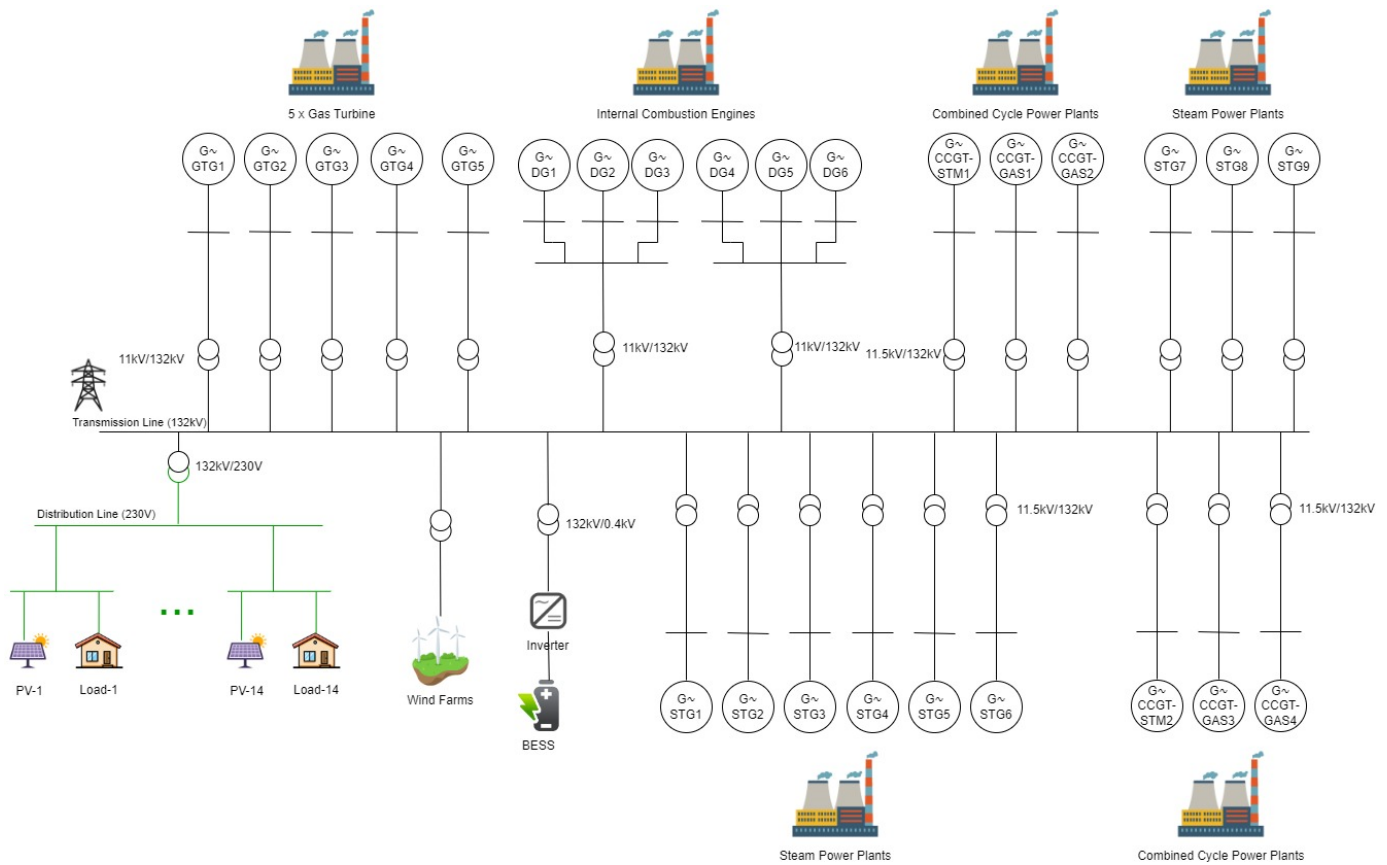


Fig. 9. Cyprus Simplified Single Line Diagram

TABLE II
UFLS SCHEME

Stage	Frequency	$PV_{shed, \%} / Load_{shed, \%}$
1	49	4%
2	48.9	4%
3	48.8	3%
4	48.7	8%
5	48.6	4%
6	48.5	4%
7	48.4	4%
8	48.3	1%
9	48.2	7%
10	48.1	6%
11	48	5%
12	47.75	9%
13	47.5	9%

TABLE III
SIMULATION PARAMETERS [28], [29]

Parameter	Value
k	1 %
ϵ	7%
δ	0.2%
Minimum kinetic energy	3000 MWs
Minimum FCR	120 MW
Normal operation	49.8-50.2 Hz
During disturbance	47-52 Hz
Post-fault steady state	49.5-50.5 Hz
ΔP	120 MW
f_{target}	48.9 & 49 Hz

TABLE IV
RESULTS WITHOUT UFLS ACCEPTED

Iteration	No. of Scenarios		FFR (MW)		Nadir (Hz)	
	Total	Filtered	Min	Max	Min	Max
1	500	485	0	0	47.69	49.27
2	485	416	4.9	33	49.04	49.17
3	416	29	3.9	26.5	49.01	49.12
4	29	0	4.9	19.2	49.1	49.12
Total	500	-	0	33	49.04	49.27

In the next iteration, the remaining 485 scenarios are simulated with the provision of FFR and all the disturbances have Nadir greater than the target. The results of the whole analysis are presented in Table. IV.

Based on the results, the correlation between Nadir and FFR power is presented in Fig. 10b, where it is obvious that there is an almost linear correlation. Furthermore, the correlation depicted in Figure 10c between ROCOF and FFR power requirements reveals a notable trend: as ROCOF decreases, there is a corresponding increase in FFR needs. However, due to the varying FCR response times and capacities across scenarios, factors independent of ROCOF, a significant dispersion exists, making it difficult the establishment of a clear correlation.

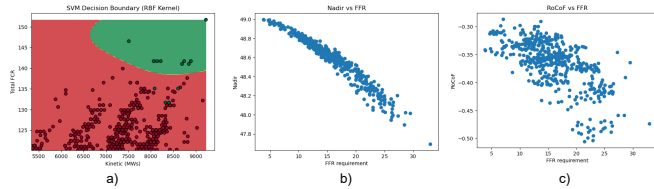


Fig. 10. No UFLS activated

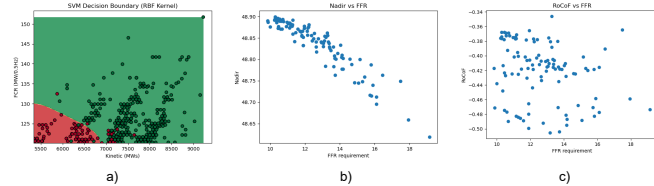


Fig. 11. 1st stage of UFLS activated

D. Results with first stage of UFLS

In this test case, the first UFLS stage is considered accepted. Hence, the target frequency is 48.9 Hz (the minimum frequency before the second stage of UFLS is activated). After simulating the same 500 random scenarios as before with only the first UFLS stage enabled, in the first iteration there were a total of 105 scenarios (represented by red dots in the Fig. 11a) where the frequency was below the target frequency. In the next iteration, BESS is activated in the system, and the requirements for FFR power range between 9.6 - 18.75 MW, and the corresponding 105 scenarios have a frequency between 48.95 - 48.98 Hz. The analytic results of the whole analysis are presented in Table. V.

In Fig. 11b, the correlation between the Nadir and the required FFR power to reach the target is presented. In comparison to the analysis without UFLS, we observe slightly larger noise but a similar linear correlation. On the contrary, no correlation between ROCOF and FFR is observed, and this is due not only to the different FCR characteristics but also to the randomness that UFLS added to the system.

TABLE V
RESULTS FOR FIRST STAGE OF UFLS ACCEPTED

Iteration	No. of Scenarios		FFR		Nadir	
	Total	Filtered	Min	Max	Min	Max
1	500	105	0	0	48.61	49.27
2	105	0	10	19	48.95	48.98
Total	500	0	0	18.75	48.95	49.27

V. CONCLUSION

This paper presented a solution to improve the stability and, mainly, the Nadir of low-inertia grids after a significant disturbance by connecting ESS to the system. The paper focused on FFR provision from ESS as the most economical method to improve Nadir and mitigate UFLS in the island systems. The FFR power sizing solution was obtained through

a simulation-based iterative method. We implemented our proposed solution in a Cyprus power system. The results verify the fast convergence and the good approach from the very first iteration, as in all scenarios, Nadir becomes greater than the target.

Future research could further develop the optimal BESS size to reduce the Nadir even closer to the target. Moreover, for the optimum planning of BESSs, a maximum power activation strategy can be developed to reduce even more the cost of operation.

ACKNOWLEDGMENT

The authors would like to thank Cyprus TSO for providing the dynamic model, which was instrumental in validating the proposed dimension methodology. Special thanks are due to Dr. Antonis Lazari and Vrahimis Koutsoloukas for their invaluable insights and support throughout this endeavor.

REFERENCES

- [1] B. J. K. et al, "Frequency control concerns in the north american electric power system," Tech. Rep. ORNL/TM-2003/41, 2002.
- [2] R. Hollinger, A. M. Cortes, and T. Erge, "Fast frequency response with bess: A comparative analysis of germany, great britain and sweden," in *2018 15th International Conference on the European Energy Market (EEM)*, 2018, pp. 1–6.
- [3] E. Ørum et al, "Future system inertia 2," Entsoe, Tech. Rep. Report Number, 2017. [Online]. Available: <http://example.com/report>
- [4] K. D. V. et al, "Dynamic dimensioning approach for operating reserves: Proof of concept in belgium," *Energy Policy*, vol. 124, pp. 272–285, 2019.
- [5] V. Knap, S. K. Chaudhary, D.-I. Stroe, M. Swierczynski, B.-I. Craciun, and R. Teodorescu, "Sizing of an energy storage system for grid inertial response and primary frequency reserve," *IEEE Transactions on Power Systems*, vol. 31, no. 5, pp. 3447–3456, 2016.
- [6] ENTSOE, "Operational reserve ad hoc team report," ENTSOE, Tech. Rep., 2012. [Online]. Available: <https://cepublicdownloads.entsoe.eu>
- [7] M. M. Michel Rezkalla, Michael Pertl, "Electric power system inertia: requirements, challenges and solutions," *Springer*, vol. 42, no. 3, pp. 2677–2693, 2018.
- [8] Z. A. O. et al, "Frequency control of future power systems: reviewing and evaluating challenges and new control methods," *MPCE*, vol. 7, no. 1, pp. 9–25, 2018.
- [9] C. K. Das, T. S. Mahmoud, O. Bass, S. Muyeen, G. Kothapalli, A. Baniyadi, and N. Mousavi, "Optimal sizing of a utility-scale energy storage system in transmission networks to improve frequency response," *Journal of Energy Storage*, vol. 29, p. 101315, 2020. [Online]. Available: <https://www.sciencedirect.com/science/article/pii/S2352152X19315646>
- [10] U. Akram, N. Mithulananthan, R. Shah, and S. Alzahrani, "Design of energy storage for frequency stability in low-inertia power grid," *IEEE Systems Journal*, vol. 17, no. 3, pp. 4763–4774, 2023.
- [11] H. Alsharif, M. Jalili, and K. N. Hasan, "Power system frequency stability using optimal sizing and placement of battery energy storage system under uncertainty," *Journal of Energy Storage*, vol. 50, p. 104610, 2022. [Online]. Available: <https://www.sciencedirect.com/science/article/pii/S2352152X22006260>
- [12] K. S. El-Bidairi, H. D. Nguyen, T. S. Mahmoud, S. Jayasinghe, and J. M. Guerrero, "Optimal sizing of battery energy storage systems for dynamic frequency control in an islanded microgrid: A case study of flinders island, australia," *Energy*, vol. 195, p. 117059, 2020. [Online]. Available: <https://www.sciencedirect.com/science/article/pii/S0360544220301663>
- [13] V. Knap, S. K. Chaudhary, D.-I. Stroe, M. Swierczynski, B.-I. Craciun, and R. Teodorescu, "Sizing of an energy storage system for grid inertial response and primary frequency reserve," *IEEE Transactions on Power Systems*, vol. 31, no. 5, pp. 3447–3456, 2016.
- [14] A. F. Ramos, I. Ahmad, D. Habibi, and T. S. Mahmoud, "Placement and sizing of utility-size battery energy storage systems to improve the stability of weak grids," *International Journal of Electrical Power and Energy Systems*, vol. 144, p. 108427, 2023. [Online]. Available: <https://www.sciencedirect.com/science/article/pii/S0142061522004392>

- [15] M. Ramírez, R. Castellanos, G. Calderón, and O. Malik, "Placement and sizing of battery energy storage for primary frequency control in an isolated section of the mexican power system," *Electric Power Systems Research*, vol. 160, pp. 142–150, 2018. [Online]. Available: <https://www.sciencedirect.com/science/article/pii/S0378779618300567>
- [16] A. Oudalov, D. Chartouni, and C. Ohler, "Optimizing a battery energy storage system for primary frequency control," *IEEE Transactions on Power Systems*, vol. 22, no. 3, pp. 1259–1266, 2007.
- [17] D. Pandit, N. Nguyen, and J. Mitra, "An analytical approach to energy storage sizing for inertia and frequency reserve support," in *2022 IEEE Power and Energy Society General Meeting (PESGM)*, 2022, pp. 1–5.
- [18] N. Nordic Analysis Group, "Requirement for minimum inertia in the nordic power system," Entsoe, Tech. Rep. Report Number, 2021. [Online]. Available: <https://www.epressi.com/media/userfiles/151043/1634122821/requirement-for-minimum-inertia-in-the-nordic-power-system.pdf>
- [19] N. M. et al, "Overview of frequency control in the nordic power system," Nordic Analysis Group, Tech. Rep., 2022. [Online]. Available: <https://www.epressi.com>
- [20] M. C. et al, "Replacement reserve for the italian power system and electricity market," *MDPI*, vol. 13, no. 2916, pp. 1566–1581, 2020.
- [21] "Fast frequency reserve – solution to the nordic inertia challenge," ENTSOE, Tech. Rep.
- [22] L. Meng, J. Zafar, S. K. Khadem, A. Collinson, K. C. Murchie, F. Coffele, and G. M. Burt, "Fast frequency response from energy storage systems—a review of grid standards, projects and technical issues," *IEEE Transactions on Smart Grid*, vol. 11, no. 2, pp. 1566–1581, 2020.
- [23] "Appendix 1 - load-frequency control and performance," ENTSOE, Tech. Rep. [Online]. Available: <https://eepublicdownloads.entsoe.eu>
- [24] F. Oyj, "Reserve products and reserve market places," FINGRID, Tech. Rep., 2023. [Online]. Available: <https://www.fingrid.fi/globalassets/dokumentit/en/electricity-market/reserves/reserve-products-and-reserve-market-places.pdf/>
- [25] E. Group, "Methodology for the dimensioning of the afrr needs," ELIA, Tech. Rep.
- [26] S. B. et al, "Ufls and smart load for frequency regulation in electrical power system: A review," *IEEE ACCESS*, vol. 11, no. 2916, pp. 110967–110984, 2023.
- [27] E. A. of Cyprus, "Pv's technical report," EAC, Tech. Rep., 2022. [Online]. Available: <https://eac.com.cy>
- [28] C. A. of Cyprus. (2023) Generation data. [Online]. Available: <https://www.eac.com.cy/EL/EAC/Operations/Pages/Generation.aspx>
- [29] T. S. O. of Cyprus, "Grid codes," TSOC, Tech. Rep., 2023. [Online]. Available: <https://tsoc.org.cy>